JOINT INSTITUTE FOR AERONAUTICS AND ACOUSTICS

NASA
National Aeronautics and Space Administration
Ames Research Center

NASA-CR-169736
19830008966

Stanford University

JIAA TR - 48

EFFECTS OF FLIGHT ON NOISE RADIATED FROM CONVECTED RING SOURCES IN COAXIAL DUAL FLOW
PART 2, THE NOISE FROM HEATED JETS

R. Dash

STANFORD UNIVERSITY
Department of Aeronautics and Astronautics
Stanford, California 94305

AUGUST 1982

ENTER:
****** AUTOMATIC END SEARCH BYPASS *****
SEARCH TITLE
DATE/FILE 12-20-83/N
***** BEGIN SEARCH BYPASS *****
DATE/FILE 12-20-83/N
PRIMARY DATA BASE ONLINE

SET NO.	NO.OF REC.	NO.OF OCC.	DESCRIPTION OF SET (+=OR, *=AND, -=NOT)
1	14	14	AU/DASH, R.
2	1719	2119	ATL/COAXIAL
	SET STATUS UTP/'DUAL FLOW'		IF00C: INVALID ARGUMENT - PROCEED
3	18	18	UTP/DUAL *+1 FLOW
4	3	6	1*2*3

DISPLAY 04/2/3

83N17237*# ISSUE 7 PAGE 1088 CATEGORY 71 RPT#: NASA-CR-169736 NAS 1.26:169736 SU-JIAA-TR-48-PT-2 CNT#: NCC2-75 82/08/00 53 PAGES
UNCLASSIFIED DOCUMENT

UTTL: Effects of flight on noise radiated from convected ring sources in coaxial dual flow. Part 2: The noise from heated jets
AUTH: A/DASH, R.
CORP: Stanford Univ., Calif. CSS: (Joint Inst. for Aeronautics and Acoustics.)
AVAIL.NTIS SAP: HC A04/MF A01
MAJS: /*AIRCRAFT ENGINES/*COAXIAL FLOW/*ENGINE NOISE/*NOISE REDUCTION
MINS: / MASS RATIOS/ RING STRUCTURES/ SOUND PROPAGATION/ TEMPERATURE PROFILES
ABA: Author
ABS: The effects of flight on noise from heated jets are discussed. The effects of the additionally, extraneously-generated dipole and simple source terms which arise as a result of the density gradients across the fluid interfaces were incorporated. The coaxial flows with inverted profiles are shown to be quieter than the conventional profiles; however, the benefit of noise reduction at higher outer-to-inner area ratios is totally offset

JIAA TR - 48

EFFECTS OF FLIGHT ON NOISE RADIATED FROM CONVECTED RING SOURCES IN COAXIAL DUAL FLOW

Part 2. The Noise From Heated Jets

R. DASH

The work presented here has been supported by the National Aeronautics and Space Administration under NASA Grant NCC 2-75.

TABLE OF CONTENTS

ABOUT THE CONTRACT AND THE PERSONNEL INVOLVED

This is a final report covering the period April 1979 to March 1982, and appears in two parts: Part 1 - The noise from unheated jets and Part 2 - The noise from heated jets.

This research was carried as part of the aeroacoustics program of the Joint Institute for Aeronautics and Acoustics, Department of Aeronautics and Astronautics, at Stanford University and was sponsored by NASA Ames Research Center under the NASA co-operative agreement contract NCC 2-75.

Professor K. Karamcheti, Director of the Institute, was the Principal Investigator of the program and Dr. R. Dash was the Chief Senior Investigator on the program. Professor I.D. Chang and Mr. Yen Liu, a Ph.D. student, also participated in the program. From NASA Ames Research Center Mr. David H. Hickey, Chief of the Low Speed Aircraft Research Branch and Mr. Adolf Atencio, Project Research Engineer, were the technical monitors for this project.

LIST OF ILLUSTRATIONS

Figure

SUMMARY

This paper is a continuation of the study described in part 1 and deals with the effects of flight on noise from heated jets. In working out this theory through the vortex sheet flow modeling, we have incorporated in our analysis the effects of the additionally, extraneously-generated dipole and simple source terms which arise as a result of the density gradients across the fluid interfaces. In addition to reasserting our earlier findings due to the effects of flight as in part 1-(i) amplification of noise in the forward quadrant, (ii) reduction of noise in the aft quadrant and (iii) no effects at $\theta = 90°$ to the jet axis—the present work shows that the coaxial flows with inverted profiles are much quieter than the conventional profiles; however, the benefit of noise reduction at higher outer-to-inner area ratios is totally offset as it (inverted profile) incurs a significant massloss and thrust-loss. Amongst all the possible coaxial configurations when one of the co-axial streams is heated—conventional profile (CP), inverted profile (IP) and the variable stream control engine (VSCE) cycle—and at constant massflow and thrust, a VSCE-cycle is the most desirable and the best possible engine cycle inasmuch as it provides over more than 18.0 dB reduction in SPL (as compared against noise from a CP-cycle) at all angles, both statically and in flight, for area ratios $\sum < 0.25$. In view of its immense potential to produce the least noise while still maintaining the constant high massflow and thrust (as of the CPcycle), the VSCE-cycle is likely to be of paramount importance in its engineering application as one of the most viable nozzles of the future. The study also further indicates that when both the coaxial streams are unequally heated, a duct-buring profile combined with the variable stream control engine (DB-VSCE) concept gives rise to another powerful coaxial device which generates the least noise, both statically and in flight,

while still maintaining the maximum massflow and thrust. In any case the duct-burning turbofan engine is simply no match with the DB-VSCE cycle inasmuch as the former is substantially noisier than the latter even at much less massflow and thrust conditions.

1. INTRINSICALLY GENERATED EXTRANEOUS SOURCES

The role played by the multipole sources in a heated jet is quite intricate and needs to be looked into carefully since it is not easy to explain their complicating role through the physics of the problem. To explain this feature, one can make use of the generalized properties of the delta function and its derivatives whereby one can show that in the presence of two or more different fluid medias having nonidentical temperatures and densities which are distinctly different at their common interface, a dipole source term may give rise to an additional simple source term and a quadrupole term may give rise to an additional dipole term plus one additional simple source term. Mani (1976a, 1976b) has utilized this idea to solve the vortex sheet modeling problem of the single round plug-flow jets. Since ours is a heated coaxial dual jet having double vortex layers, it will be worthwhile to show that by utilizing this delta function technique one can find additional dipole and simple source terms generated from the quadrupole-type ring sources. These additionally generated source terms must be taken into consideration before one works out the final radiation from the heated coaxial flow through the ring modeling.

Let us now consider the original equations which govern the wave propagation of the radiations from the two axisymmetric ring sources (without any periodicity n along ϕ) in the heated coaxial flow which we write as:

$$\frac{1}{c_p^2}\left(\frac{\partial}{\partial t}+U_p\frac{\partial}{\partial z}\right)^2 p-\nabla^2 p=\rho_p(r)L_j\left\{\frac{\delta(r-r_0)}{r}\delta(z-U_c t)e^{-i\omega t}\right\} \qquad (1)$$

inside the primary flow $0\le r\le r_p$

$$\frac{1}{c_s^2}\left(\frac{\partial}{\partial t}+U_s\frac{\partial}{\partial z}\right)^2 p-\nabla^2 p=\rho_s(r)\mathcal{L}_j\left\{\frac{\delta(r-r_0)}{r}\delta(z-U_c t)e^{-i\omega t}\right\} \qquad (2)$$

inside the secondary flow $r_p\le r\le r_s$

$$\frac{1}{c_f^2}\left(\frac{\partial}{\partial t}+U_f\frac{\partial}{\partial z}\right)^2 p-\nabla^2 p=0, \qquad (3)$$

inside the flight simulating ambient flow $r_s\le r$

Before we explain mathematically as to how the additional source terms are intrinsically generated within the system, let us look at the multiplication property of the differentiated generalized function in conjunction with another fixed function ϕ which has continuous derivatives at least up to the nth order on a neighbourhood of the origin (see Hoskins (1979)),

$$\Phi(\tau)\delta^n(\tau)=\Phi(0)\delta^n(\tau)-{}^nC_1\Phi'(0)\delta^{n-1}(\tau)+{}^nC_2\Phi''(0)\delta^{n-2}(\tau)+\cdots\cdots+\cdots\cdots+(-1)^n\Phi^n(0)\delta(\tau) \qquad (4)$$

This formula will be made use of when the higher order multipole-sources act as the driving sources and appear on the right hand side of the wave equations. Since we concern ourselves with the quadrupole-type sources we may use only up to the first three lower order products involving the δ-function which we write:

$$\Phi(\tau)\,\delta(\tau) = \Phi(0)\,\delta(\tau)$$

$$\Phi(\tau)\,\delta'(\tau) = \Phi(0)\,\delta'(\tau) - \Phi'(0)\,\delta(\tau)$$

$$\Phi(\tau)\,\delta''(\tau) = \Phi(0)\,\delta''(\tau) - 2\,\Phi'(0)\,\delta'(\tau) + \Phi''(0)\,\delta(\tau) \qquad (5)$$

where the dashes denote differentiation with respect to the argument. Making use of the foregoing relations in equation (5) and the coordinate relations defined in equation (61) of part 1) one can write for the x-x quadrupole component of the source term in equation (2) as:

$$a_{11} = \rho_s(r)\,\frac{\partial^2}{\partial x^2}\left\{\frac{\delta(r-r_0)}{r}\,\delta(z-v_c t)\,e^{-i\omega t}\right\}$$

$$= \rho_s(r_0)\left(\frac{\partial^2}{\partial x^2}\delta_s\right) - 2\left(\frac{\partial \rho_s(r)}{\partial x}\right)_{r_0,\phi}\left(\frac{\partial \delta_s}{\partial x}\right) + \left(\frac{\partial^2 \rho_s(r)}{\partial x^2}\right)_{r_0,\phi}\delta_s \qquad (6)$$

$$=$$

$$= \rho_s(r_0)\left[\cos^2\phi\left(\frac{\partial^2\delta_s}{\partial r^2}\right) + \frac{\sin^2\phi}{r_0}\left(\frac{\partial\delta_s}{\partial r}\right)\right]_{r_0} - 2\cos^2\phi\left(\frac{d\rho_s(r)}{dr}\right)_{r_0}\left(\frac{\partial\delta_s}{\partial r}\right)_{r_0}$$

$$+\left[\cos^2\phi\left(\frac{d^2\rho_s(r)}{dr^2}\right) + \frac{\sin^2\phi}{r_0}\left(\frac{d\rho_s(r)}{dr}\right)\right]\delta_s \qquad (7)$$

As one can notice in equation (7), the differentiations are evaluated at $r = r_0$. This is due to the fact that the appropriate radiations can be derived from the simple source result, due to the simple source term $\delta_s = \frac{\delta(r-r_0)}{r}\delta(z-U_c t)\,e^{-i\omega t}$ by differentiating the simple source result with respect to the source coordinate which in the present case is $r = r_0$, for the ring source located in the secondary stream of the coaxial jet. The emergence of equation (7) from its preceding step has been made possible due to the presence of density gradients across the fluid interface at $r = r_s$ which separates the secondary stream from the ambience which simulates flight. It is well known that the sources of noise are principally generated in and around the secondary/ambient interface, although for sake of convenience we tactfully replaced them by putting a ring source in the midst of the secondary stream at $r = r_0$. Therefore, the density gradients suffixed with r_0 essentially reflect the density gradients at $r = r_s$ where they really exist. We will come to this point again at a later stage.

Now replacing the density gradients as:

$$\frac{d\rho_s(r)}{dr} = \rho_s'(r)$$

$$\frac{d^2\rho_s(r)}{dr^2} = \rho_s''(r) \qquad (8)$$

and rearranging the terms in equation (7), one can have explicit expressions for the quadrupole component a_{11} and also for other quadrupole components (following exactly similar procedure) which we write as:

$$a_{11} = \cos^2\phi\left[\rho_s(r_0)\left(\frac{\partial^2\delta_s}{\partial r^2}\right)_{r_0} - 2\rho_s'(r_0)\left(\frac{\partial\delta_s}{\partial r}\right)_{r_0} + \rho_s''(r_0)\,\delta_s\right] + \frac{\sin^2\phi}{r_0}\left[\rho_s(r_0)\left(\frac{\partial\delta_s}{\partial r}\right)_{r_0} + \rho_s'(r_0)\,\delta_s\right] \tag{9}$$

$$a_{22} = \sin^2\phi\left[\rho_s(r_0)\left(\frac{\partial^2\delta_s}{\partial r^2}\right)_{r_0} - 2\rho_s'(r_0)\left(\frac{\partial\delta_s}{\partial r}\right)_{r_0} + \rho_s''(r_0)\,\delta_s\right] + \frac{\cos^2\phi}{r_0}\left[\rho_s(r_0)\left(\frac{\partial\delta_s}{\partial r}\right)_{r_0} + \rho_s'(r_0)\,\delta_s\right] \tag{10}$$

$$a_{33} = \rho_s(r_0)\,\frac{\partial^2\delta_s}{\partial z^2} \tag{11}$$

$$a_{12} = \frac{\sin 2\phi}{2}\,\rho_s(r_0)\left[\left(\frac{\partial^2\delta_s}{\partial r^2}\right)_{r_0} - \frac{1}{r_0}\left(\frac{\partial\delta_s}{\partial r}\right)_{r_0}\right] - \sin 2\phi\,\rho_s'(r_0)\left(\frac{\partial\delta_s}{\partial r}\right)_{r_0} + \frac{\sin 2\phi}{2}\left[\rho_s''(r_0) - \frac{1}{r_0}\rho_s'(r_0)\right]\delta_s \tag{12}$$

$$a_{13} = \cos\phi\left[\rho_s(r_0)\left(\frac{\partial^2\delta_s}{\partial r\,\partial z}\right)_{r_0} - \rho_s'(r_0)\,\frac{\partial\delta_s}{\partial z}\right] \tag{13}$$

$$a_{13} = \sin\phi\left[\rho_s(r_0)\left(\frac{\partial^2\delta_s}{\partial r\,\partial z}\right)_{r_0} - \rho_s'(r_0)\,\frac{\partial\delta_s}{\partial z}\right] \tag{14}$$

Equation (6) shows that the x-x quadrupole resolves into a purely quadrupole term proportional to the local density of the stream plus one transvers dipole term proportional to the local density gradient and one simple source term proportional to the second-order local density gradient. However, when the x-x quadrupole is expressed in terms of polar coordinates, the scenario looks different. In terms of polar coordinates, one finds (see equation 9) that it resolves into a quadrupole in the radial direction proportinal to $\rho_s(r_0)\cos^2\phi$, plus one radial dipole term proportional to and one simple source proportional to $\left[\rho_s(r_0)\frac{\sin^2\phi}{r_0} - 2\rho_s'(r_0)\cos^2\phi\right]$. Similar interpretation can be provided for the y-y quadrupole in equation (10). The purely axial z-z quadrupole (see equation 11) remains unaffected and generates no lower order singularities because of the absence of any mean density gradients in the axial direction. The x-y quadrupole in equation (12) provides one radial quadrupole proportional to $\rho_s(r_0)\sin\phi\cos\phi$, plus one radial dipole term proportional to $\sin 2\phi\left(-\frac{1}{2r_0}\rho_s(r_0) - \rho_s'(r_0)\right)$ and one simple source term roportional to $\sin\phi\cos\phi\left(\rho_s''(r_0) - \frac{1}{r_0}\rho_s'(r_0)\right)$. The x-z quadrupole in eqation (13) provides one r-z type quadrupole proportional to $\rho_s(r_0)\cos\phi$ and one axial-type dipole proportioal to $-\rho_s'(r_0)\cos\phi$. Similar interpretation is obvious for the y-z quadrupole in equation (14).

Following the approach shown in Mani's work (1976b) on heated jet noise from single round jets, and recognizing the fact that the density gradients at $r = h_o$ really mean the density gradients across the fluid interface at $r = r_s$ where they physically exist, one can write them empirically as:

$$\left(\frac{d\rho_s(r)}{dr}\right)_{h_o} = \rho_s'(r_o) = \frac{\rho_f - \rho_s}{r_s} St_2$$

$$\left(\frac{d^2\rho_s(r)}{dr^2}\right)_{h_o} = \rho_s''(r_o) = \frac{\rho_f - \rho_s}{r_s^2} St_2^2 \qquad (15)$$

The quantity $\rho_s(h_o)$ is actually the density of the fluid in the secondary stream and as such:

$$\rho_s(r_o) = \rho_s \qquad (16)$$

Following exactly the same procedure we can find out parallel expressions for the quadrupole components of the ring-source in the primary flow which represents the acoustic sources generated at the primary/secondary interface at $r = r_p$ where again the density gradients $\frac{d\rho_p(r)}{dr}, \frac{d^2\rho_p(r)}{dr^2}$ exist. Now writing down those expressions we have:

$$b_{11} = \cos^2\phi \left[\rho_p(r_o)\left(\frac{\partial^2\delta_p}{\partial r^2}\right)_{r_o} - 2\rho_p'(r_o)\left(\frac{\partial\delta_p}{\partial r}\right)_{r_o} + \rho_p''(r_o)\,\delta_p\right]$$

$$+ \frac{\sin^2\phi}{r_o}\left[\rho_p(r_o)\left(\frac{\partial\delta_p}{\partial r}\right)_{r_o} + \rho_p'(r_o)\,\delta_p\right] \qquad (17)$$

$$b_{22} = \sin^2\phi \left[\rho_p(r_0) \left(\frac{\partial^2 \delta_p}{\partial r^2} \right)_{r_0} - 2\rho_p'(r_0) \left(\frac{\partial \delta_p}{\partial r} \right)_{r_0} + \rho_p''(r_0)\, \delta_p \right] + \frac{\cos^2\phi}{r_0} \left[\rho_p(r_0) \left(\frac{\partial \delta_p}{\partial r} \right)_{r_0} + \rho_p'(r_0)\, \delta_p \right] \tag{18}$$

$$b_{33} = \rho_p(r_0) \frac{\partial^2 \delta_p}{\partial z^2} \tag{19}$$

$$b_{12} = \frac{\sin 2\phi}{2} \rho_p(r_0) \left[\left(\frac{\partial^2 \delta_p}{\partial r^2} \right)_{r_0} - \frac{1}{r_0} \left(\frac{\partial \delta_p}{\partial r} \right)_{r_0} \right] - \sin 2\phi\, \rho_p'(r_0) \left(\frac{\partial \delta_p}{\partial r} \right)_{r_0} + \frac{\sin 2\phi}{2} \left[\rho_p''(r_0) - \frac{1}{r_0} \rho_p'(r_0) \right] \delta_p \tag{20}$$

$$b_{13} = \cos\phi \left[\rho_p(r_0) \left(\frac{\partial^2 \delta_p}{\partial r \partial z} \right)_{r_0} - \rho_p'(r_0) \frac{\partial \delta_p}{\partial z} \right] \tag{21}$$

$$b_{23} = \sin\phi \left[\rho_p(r_0) \left(\frac{\partial^2 \delta_p}{\partial r \partial z} \right)_{r_0} - \rho_p'(r_0) \frac{\partial \delta_p}{\partial z} \right] \tag{22}$$

where

$$\rho_p(r_0) = \rho_p$$

$$\left(\frac{d\rho_p(r)}{dr}\right)_{r_0} = \rho_p'(r_0) = \frac{\rho_s - \rho_p}{r_p} St_1$$

$$\left(\frac{d^2\rho_p(r)}{dr^2}\right)_{r_0} = \rho_p''(r_0) = \frac{\rho_s - \rho_p}{r_p^2} St_1^2$$

$$\delta_p = \frac{\delta(r-r_0)}{r} \delta(z - U_c t) e^{-i\omega t} \tag{23}$$

2. RADIATION FROM SOURCES IN THE HOT SECONDARY STREAM

While working out the radiation problem for a cold coaxial flow in part 1, the primary and secondary stream densities were purposefully kept distinctly different, even though when finding the actual radiation for the cold jet we had to make $\rho_p = \rho_s = \rho_f = \rho_0$, same as the normal ambient density. Thus fundamentally the radiation expressions found earlier are valid for both the hot and cold situations. However, when making applications of those fundamental results to a hot flow situation, one has to be careful so as to bear in mind that it is not the only radiation from the only soruce which was thought to be existing alone in isolation and that meanwhile because of the emergence of additional source terms generated due to the presence of temperature/density gradients across the fluid interfaces, appropriate additional radiations from these extraneous sources must be taken into account. This is an inevitable consequence for a flow where there is difference in its flow parameters (like temperature and denisty) from its surrounding fluid.

In view of the above consideration and recognizing that a differentiation of a field due to a simple source representation on the right hand side of a wave equation with respect to source coordinates yields an appropriate multipole source radiation, one can make use of equations (37, 55-57) of part 1 in equation (9-14), to get the radiation expressions for a quadrupole-type axisymmetric ring source (free from any periodicity n along ϕ) in a hot secondary stream which we write as follows:

$$a_{11} = \frac{\rho_s \mathcal{K}_s}{i\pi r_s h_o}\left[\left\{\frac{\mathcal{K}_s h_o (C_o - C_2)}{2} - 2\left(\frac{\rho_f}{\rho_s} - 1\right) St_2 \frac{h_o}{r_s}\left[C_1 + \frac{St_2 \cdot C_o}{2\mathcal{K}_s r_s}\right]\right\}\cos^2\phi + \left\{C_1 - \left(\frac{\rho_f}{\rho_s} - 1\right)\frac{St_2 \cdot C_o}{\mathcal{K}_s r_s}\right\}\sin^2\phi\right] \frac{\exp i\{\mathcal{R} k \omega/c_f - \omega t\}}{\mathcal{R}\left[1 - \omega/c_f (M_c - M_f)\cos\theta\right]}$$

$$a_{22} = \frac{\rho_s \mathcal{K}_s}{i\pi r_s h_o}\left[\left\{\frac{\mathcal{K}_s h_o (C_o - C_2)}{2} - 2\left(\frac{\rho_f}{\rho_s} - 1\right) St_2 \frac{h_o}{r_s}\left[C_1 + \frac{St_2 \cdot C_o}{2\mathcal{K}_s r_s}\right]\right\}\sin^2\phi + \left\{C_1 - \left(\frac{\rho_f}{\rho_s} - 1\right)\frac{St_2 \cdot C_o}{\mathcal{K}_s r_s}\right\}\cos^2\phi\right] \frac{\exp i\{\mathcal{R} k \omega/c_f - \omega t\}}{\mathcal{R}\left[1 - \omega/c_f (M_c - M_f)\cos\theta\right]}$$

$$a_{33} = \frac{\rho_s}{i\pi r_s}\left(k\,\omega/c_f\right)^2 \cos^2\theta \; \frac{C_o \exp\{i\mathcal{R} k \omega/c_f - \omega t\}}{\mathcal{R}\left[1 - \omega/c_f (M_c - M_f)\cos\theta\right]^3}$$

$$a_{12} = \frac{\rho_s \mathcal{K}_s}{i\pi r_s h_o} \sin\phi\cos\phi \left[\frac{\mathcal{K}_s h_o (C_o - C_2)}{2} - 2\left(\frac{\rho_f}{\rho_s} - 1\right) St_2 \frac{h_o}{r_s}\left[C_1 + \frac{St_2 C_o}{2\mathcal{K}_s r_s} - C_1 + \left(\frac{\rho_f}{\rho_s} - 1\right)\frac{St_2 \cdot C_o}{\mathcal{K}_s r_s}\right]\right] \frac{\exp i\{\mathcal{R} k \omega/c_f - \omega t\}}{\mathcal{R}\left[1 - \omega/c_f (M_c - M_f)\cos\theta\right]}$$

$$a_{13} = \frac{\rho_s}{\pi r_s} k\, c_0/c_f \cos\theta \cos\phi \left[\mathcal{K}_s C_1 + \left(\frac{\rho_f}{\rho_s} - 1\right) \frac{St_2 \cdot C_0}{r_s} \right] \cdot \frac{\exp i\{\mathcal{R} k\, c_0/c_f - \omega t\}}{\mathcal{R}\left[1 - c_0/c_f (M_c - M_f) \cos\theta\right]^2}$$

$$a_{23} = \frac{\rho_s}{\pi r_s} k\, c_0/c_f \cos\theta \sin\phi \left[\mathcal{K}_s C_1 + \left(\frac{\rho_f}{\rho_s} - 1\right) \frac{St_2 \cdot C_0}{r_s} \right] \cdot \frac{\exp i\{\mathcal{R} k\, c_0/c_f - \omega t\}}{\mathcal{R}\left[1 - c_0/c_f (M_c - M_f) \cos\theta\right]^2} \qquad (24)$$

It is worthwhile to point out although the above results are valid for a hot jet case, we can also derive from them the corresponding results for a cold jet case (see equation (62) of part 1) simply by putting $\rho_s/\rho_f = 1$ in the relations given in equation (24).

Making use of the formulas in equations (53) and (54) of part 1, one can find from equation (24) the far-field radiation due to a quadrupole type ring source in the hot secondary stream of a coaxial dual flow as:

$$I_{rhs} = \langle \bar{a}_{33}^2 \rangle + 2\langle \bar{a}_{11}^2 \rangle + 2\langle \bar{a}_{12}^2 \rangle + 4\langle \bar{a}_{13}^2 \rangle$$

$$= \left(\frac{\rho_s}{\pi R r_s h_0}\right)^2 \frac{1}{Q_2^2 |\delta_2|^2} \left\{ \frac{|\gamma_0|^2 \lambda_{3s}^2 (c_0/c_f)^4 \cos^4\theta}{Q_2^2 |M_2|^2} \right.$$

$$+ \left| \frac{3}{4} A_2^2 + \frac{3}{4} B_2^2 + \frac{A_2 B_2}{2} \right|$$

$$+ \frac{1}{4} \left| A_2 - B_2 \right|^2$$

$$\left. + \frac{2|2\gamma_1 - B_2|^2 \lambda_{3s}^2 \cdot (c_0/c_f)^2 \cos^2\theta}{Q_2^2} \right\} \qquad (25)$$

where

$$A_1 = \frac{\chi_2(\gamma_0 - \gamma_2)}{2} - (P_2 - 1) St_2 \cdot \left(1 + \frac{1}{\sqrt{1+\Sigma}}\right)\left[\gamma_1 + \frac{\gamma_0 \cdot St_2}{2 w_2}\right]$$

$$B_2 = \gamma_1 - (P_2 - 1)\frac{\gamma_0 \cdot St_2}{w_2} \qquad (26)$$

These variables have already been defined in part 1 while dealing whith the cold jet radiation from the coaxial jet.

Here again it is interesting to point out thay by putting P_2 one can reduce the hot radiation results of equation (26) to the cold radiation results in equation (63) of part 1, when there is an axisymmetric ring source in the secondary stream.

3. RADIATION FROM SOURCES IN THE HOT PRIMARY STREAM

Following the reasoning as in section 2, and making use of the equations (78, 87-89) of part 1 in equaitons (17-22) one can obtain the radiation expressions for a quadrupole-type axisymmetric ring source (free from any periodicity n along ϕ) in a hot primary stream which we write as follows:

$$b_{11} = \frac{2\rho_p K_p}{i\pi^2 r_s r_p r_0}\left(\frac{A_1 \cos^2\phi + B_1 \sin^2\phi}{G_0}\right)\frac{\exp i\{Rk\,c_0/c_f - \omega t\}}{R[1 - c_0/c_f (M_c - M_f)\cos\theta]}$$

$$b_{22} = \frac{2\rho_p K_p}{i\pi^2 r_s r_p r_0}\left(\frac{A_1 \sin^2\phi + B_1 \cos^2\phi}{G_0}\right)\frac{\exp i\{Rk\,c_0/c_f - \omega t\}}{R[1 - c_0/c_f (M_c - M_f)\cos\theta]}$$

$$b_{33} = \frac{2\rho_p}{i\pi^2 r_s r_p}\frac{(k\,c_0/c_f)^2 \cos^2\theta}{G_0} J_0(K_p r_0)\frac{\exp i\{Rk\,c_0/c_f - \omega t\}}{R[1 - c_0/c_f (M_c - M_f)\cos\theta]^3}$$

$$b_{12} = \frac{2\rho_p K_p}{i\pi^2 r_s r_p r_0}\frac{\sin\phi\cos\phi}{G_0}(A_1 - B_1)\frac{\exp i\{Rk\,c_0/c_f - \omega t\}}{R[1 - c_0/c_f (M_c - M_f)\cos\theta]}$$

$$b_{13} = \frac{2\rho_p K_p}{\pi^2 r_s r_p}\frac{k\,c_0/c_f \cos\theta\cos\phi}{G_0}\left[2J_1(K_p r_0) - B_1\right]\cdot$$

$$\cdot\frac{\exp i\{Rk\,c_0/c_f - \omega t\}}{R[1 - c_0/c_f (M_c - M_f)\cos\theta]^2}$$

$$b_{23} = \frac{2\rho_p K_p}{\pi^2 r_s r_p} \frac{k\, c_0/c_f \cos\theta \sin\phi}{G_0} \left[2 J_1(K_p r_0) - B_1 \right] \cdot \frac{\exp i\{Rk\, c_0/c_f - \omega t\}}{R\left[1 - c_0/c_f (M_c - M_f)\cos\theta\right]^2} \qquad (27)$$

where

$$A_1 = \frac{K_p r_0}{2}\left[J_0(K_p r_0) - J_2(K_p r_0)\right] - 2\left(\frac{\rho_s}{\rho_p} - 1\right) St_1 \cdot \frac{r_0}{r_p} J_1(K_p r_0) - \left(\frac{\rho_s}{\rho_p} - 1\right) St_1^2 \cdot \frac{r_0}{r_p} \frac{J_0(K_p r_0)}{K_p r_p}$$

$$B_1 = J_1(K_p r_0) - \left(\frac{\rho_s}{\rho_p} - 1\right) St_1 \cdot \frac{J_0(K_p r_0)}{K_p r_p} \qquad (28)$$

In the absence of any density gradients across the fluid interface one can put $\rho_s/\rho_p = 1$ in the above set of equations in (27-28) to recover the rediation results for the cold jet case and the reduced results will be exactly the same as given in equation (91) of part 1.

To find the far field radiation from the axisymmetric ring source (free from any periodicity along ϕ) in the hot primary stream, we make use of the formulas in equations (53) and (54) of part 1 and also the foregoing relations in equation (27-28) which yield:

$$I_{rhp} = \langle \bar{b}_{33}^2 \rangle + 2\langle \bar{b}_{11}^2 \rangle + 2\langle \bar{b}_{12}^2 \rangle + 4\langle \bar{b}_{13}^2 \rangle$$

$$= \left(\frac{2\rho_p}{\pi^2 R r_s r_p}\right)^2 \frac{1}{|M_2 \delta_1|^2} \left\{ \frac{(c_0/c_f)^4 \cos^4\theta}{Q_1^2} \left| \frac{J_0(x_1)}{M_1} \right|^2 \right.$$

$$+ \frac{1}{\lambda_{3p}^2} \left| \frac{3}{4} A_1^2 + \frac{3}{4} B_1^2 + \frac{A_1 B_1}{2} \right|$$

$$+ \frac{1}{4\lambda_{3p}^2} \left| A_1 - B_1 \right|^2$$

$$\left. + \frac{2(c_0/c_f)^2 \cos^2\theta}{Q_1^2} \left| 2J_1(x_1) - B_1 \right|^2 \right\} \qquad (29)$$

where we rewrite A_1 and B_1 in equation (29) in a different form as:

$$A_1 = \frac{x_1}{2}\left[J_0(x_1) - J_2(x_1)\right] - \left(\frac{P_1}{P_2} - 1\right) St_1 \cdot \left[J_1(x_1) + St_1 \frac{J_0(x_1)}{2u_1}\right]$$

$$B_1 = J_1(x_1) - \left(\frac{P_1}{P_2} - 1\right) St_1 \frac{J_0(x_1)}{u_1} \qquad (30)$$

The hot jet radiaiton result in equation (29) can be easily reduced to produce the cold jet radiation result in equation (92) of part 1 simply by putting $P_1 = P_2 = 1$ in equation (30).

4. INTENSITY OF RADIATION DUE TO RING SOURCES IN HOT COAXIAL DUAL FLOW AND APPLICATION OF THE THEORY

Since the problem considered here is a linear one we apoly the principle of superposition according to which we must combine the intensities of radiation due to both the ring-sources in the hot secondary and in the hot primary streams of the heated coaxial dual flow. In view of this we now combine the results of equations (25) and (29) to obtain the total far-field intensity which is expressed as:

$$I = \left(\frac{\rho_f}{R}\right)^2 \frac{64(1+\Sigma)}{\pi^4 D^4}\left[\frac{RHP}{P_1^2} + \left(\frac{\pi}{1+\sqrt{1+\Sigma}}\right)^2 \frac{RHS}{P_2^2}\right]$$

where

(31)

$$RHP = \frac{1}{|M_2\delta_1|^2}\left\{\frac{(\omega/c_f)^4 \cos^4\theta}{Q_1^2}\left|\frac{J_0(x_1)}{M_1}\right|^2 + \frac{1}{\lambda_{3p}^2}\left|\frac{3}{4}A_1^2 + \frac{3}{4}B_1^2 + \frac{A_1B_1}{2}\right| + \frac{1}{4\lambda_{3p}^2}\left|A_1 - B_1\right|^2 + \frac{2(\omega/c_f)^2\cos^2\theta}{Q_1^2}\left|2J_1(x_1) - B_1\right|^2\right\} \quad (32)$$

$$RHS = \frac{1}{|Q_2 \delta_1|^2} \left\{ \frac{|\gamma_0|^2 \lambda_{3s}^2 \cdot (c_0/c_f)^4 \cos^4\theta}{Q^2 |M_2|^2} \right.$$

$$+ \left| \frac{3}{4} A_2^2 + \frac{3}{4} B_2^2 + \frac{A_2 B_2}{2} \right|$$

$$+ \frac{1}{4} \left| A_2 - B_2 \right|^2$$

$$\left. + \frac{2 |2\gamma_1 - B_2|^2 \lambda_{3s}^2 \cdot (c_0/c_f)^2 \cos^2\theta}{Q_2^2} \right\} \qquad (33)$$

Here again for convenience of handling the problem and in order to keep the complexity of the algebra to a minimum we have considered a situation when the centers of the ring sources perfectly coalesce so as to emit radiation to reach the observer simultaneously in which case $R = \mathcal{R}$ and θ, the angle of emission at the retarded time, is the same for both.

To illustrate the above theory, the variation in intensity of acoustic radiation, expressed in decibels, is shown as a function of flow Mach numbers (M_p, M_s), flight Mach numbers (M_f), flow densities (P_1, P_2), outer-to-inner area ratios (Σ), outer-to-inner velocity ratios (Γ) and Strouhal numbers which, unless otherwise stated, have been considered at $St_1 = 0.2$, $St_2 = 0.2$. This represents the combined radiation due to all the nine quadrupole components of the ring source in the primary flow plus that due to all the nine quadrupole components of the ring source in the secondary flow. One of the most salient features of the coaxial flows discussed here is the comparison and assessment of the acoustic perfomance of different modes of operation: a) cold-inner/cold-outer, b) cold-inner/hot-outer, c) hot-inner/ cold-outer

and d) hot-inner/hot-outer. The change in intensity level is analyzed in the following figures by a plot of variation in intensity level with direction θ (measured from the direction convection) and with flight Mach number M_f. The quantity plotted is the directional intensity and is expressed in terms of the sound pressure level, decibels (dB), where:

$$dB = 10 \log_{10} I(M_f) \tag{34}$$

$$I(M_f) = \frac{64}{\pi^4}(1+\Sigma)\left[\frac{RHP}{P_1^2} + \left(\frac{\pi}{1+\sqrt{1+\Sigma}}\right)^2 \frac{RHS}{P_2^2}\right] \tag{35}$$

The parameters P_1 and P_2 may take on any value to reflect any mode of operation. When $P_1 = P_2 = 1$, it is a cold-inner/cold-outer mode at ambient temperature at 288 K; when $P_1 = P_2 = 4$, it is a hot-inner/hot-outer mode at a very hot temperature of 1152K ; when $P_1 = 1$ and $P_2 = 4$, it is an inner-cold/outer-hot flow at inner temperature 288K and outer (hot) temperature of 1152K; when $P_1 = 4$, $P_2 = 1$, it is an inner-hot/outer-cold flow at inner (hot) temperature of 1152K and outer temperature of 288K. When $P_2 = 2$, it represents a moderately hot outer flow at temperature 576K.

In figures 1(a-d), a comparison is made of the variation of intensity levels due to all the four possible modes of operation, at outer-to-inner area ratios $\Sigma = 1$, 4, 10 and 20. In all these plots, we have shown the variation at higher angles to the jet axis (more than 30°) of importance in

flight. The thrust and massflow in each figure is maintained constant for all these modes. All these figures show that thrust and massflow remaining constant, an inner-cold/outer-cold made is the least noisy and an inner-hot/outer-cold mode is the most noisy. And in general, for noise suppression point of view, an inner-cold/outer-cold mode is the most desirable and in order of preference it is followed by an inner-hot/outer-hot mode, an inner-cold/outer-hot mode and lastly by an inner-hot/outer-cold mode which is the worst mode of operation from acoustic point of view. This is also one of the major findings of the experimental studies on supersonic jet noise suppression by coaxial cold/heated jets by Dosanjh et al (1976). However, one must remember that even though an inner-cold/outer-cold mode of operation offers the best noise suppression, it is not the practical engine cycle. Since for practical applications of the coaxial jet scheme for jet noise suppression, it is essential that at least one of the component jet streams be heated, it is then most desirable to heat the annular/secondary streams of the coaxial configuration if the overall levels of the radiated noise at all angles are to be attenuated. As far as the inner-hot/outer-hot combination is concerned, the plots show that in order to generate the same amount of thrust as the other combinations, a very high-temperature coaxial jet must be operated under very high-speed conditions and this will eventually give rise to other kinds of noise associated with the high-speed flows which need to be treated differently. Anyway, this kind of coaxial combination is not a practical engine cycle and also not in use.

Figures 2(a-d) show the variation of radiation when the inner stream and the outer stream are operated at $M_p = 0.5$, $M_s = 0.9$. This is an inverted velocity profile jet but under different temperature and thrust conditions.

These plots again show that an inner-cold/outer-cold stream is not only the least noisy but also has the maximum thrust and massflow. An inner-hot/outer-cold coaxial stream which has the second maximum thrust (after the inner-cold/outer-cold) produces the utmost noise; an inner-hot/outer-hot mode produces the minimum thrust and the inner-cold/outer-hot mode produces somewhat better thrust, but comparatively more noise. As the outer-to-inner area raito (Σ) increases, the thrust and the massflow due to the inner-cold/outer-cold mode and the inner-hot/outer-cold mode increase substantially, whereas those due to an inner-hot/outer-hot mode increase very slowly. On the other hand, the thrust and the massflow due to an inner-cold/outer-hot mode gradually decrease as a result of increasing area ratio which also enhances noise due to all modes at all angles. Since the meaningful comparisons come when the massflow and thrust are constant, and since the fully cold and fully hot coaxial streams are not very practical engine cycles, let us now turn to the ones which are of real relevance in their engineering applications.

Thus we are now left with two possible types of coaxial configurations: one where either of the two streams is heated and the other where both the streams are unequally heated. Figures 3(a-d) illustrate the variation in the intensity of radiation when one of the streams is heated and they compare the sound pressure levels, SPL(dB), due to three different coaxial combinations: Conventional Profile (CP), Inverted Profile (IP) and the Variable Stream Control Engine (VSCE)-cycle. In the case of a conventional profile (CP) it represents a coaxial configuration where the flow pattern consists of a hot,

high speed inner flow combined with a cold, low speed outer flow. The inverted profile (IP) which is a combination of the iverted velocity profile and inverted temperature profile represents a coaxial configuration where the flow pattern consists of a cold, low speed inner flow combined with a hot, high speed outer flow. As far as the definitions are concerned, an inverted profile and a conventional profile can be easily interconverted simply by interchanging their respective velocities and temperatures, without in any way disturbing the cross-sectional areas of the inner and the outer streams. It is worthwile to remark that the inverted profile may have a somewhat different connotation in its applied (industrial) sense insofar as in actual engineering applications the concept of area inversion is associated with the inversion of the flow quantities. However, as far as this study is concerned an inverted profile may be regarded as one which, as defined eariler, represents a cold, low speed inner/hot, high speed outer situation. Finally, the variable stream control engine (VSCE)-cycle which represents a coaxial configuration where everything of a regular, conventional profile—including velocity, temperature and cross-sectional areas—is completely inverted, implying thereby the complete interchange of velocity, temperature and cross-sectional area of one stream with the other. In the process of inversion from a conventional profile to a variable stream control engine cycle, we find that both the massflow and thrust remain constant at all outer-to-inner area ratios Σ= 1, 4, 10 and 20. Strictly speaking a variable stream control engine cycle is the one which has the capability of being switched to and fro between itself and a conventional profile cycle while maintaining the inherent massflow and thrust constant. With these definitions of an IP-cycle, CP-cycle and VSCE-cycle, let us now turn our

attention to Figure 3(a) where one notices that at $\Sigma = 1$, the IP and VSCE-cycles become one and the same and that at practically all angles of interest shown therein, the IP (and also VSCE)-cycle is at least 6dB quieter in SPL than the CP-cycle, at constant massflow and constant thrust. This benefit in noise reduction is retained both statically as well as in flight. Figures 3(b)-3(d) show the above comparison at $\Sigma = 4$, 10 and 20 respectively. In all these figures, the VSCE-cycle and the CP-cycle maintain the same massflow and thrust, whereas the IP-cycle suffers from massloss and thrustloss as compared to the amount of massflow and thrust due to the CP-cycle. And this massloss and thrustloss worsens as we move to the higher area ratios (Σ). In other words, as we move from $\Sigma = 1$ to $\Sigma = 4$, 10, 20, the IP-cycle suffers increased massloss and increased thrust-loss. On the other hand, the CP- and VSCE-cycles maintain the same constant massflow and thrust at all values of outer-to-inner area ratios Σ. However, it has to be noted that unlike the IP-cycle, their (i.e. CP and VSCE) massflow and thrust increases as the area ratio increases. At $\Sigma = 4$ to 20, the plots show that the IP-cycle provides reduction of noise at all angles, compared to a CP-cycle, and that as one moves from static ($M_f = 0$) to a flight situation, $M_f = 0.3$, or 0.6, the amount of noise reduction already derived in the static case somewhat slightly diminishes in the forward quadrant ($\pi/2 < \theta < \pi$) and remains unchanged in the aft quadrant ($0 < \theta < \pi/2$). To put this in a simpler way, one can say that the static benefit of noise reduction due to an IP-cycle is somewhat lost in the forward quadrant due to flight, while this benefit is well maintained in the aft quadrant due to flight. Furthermore, this loss in the static benefit in the forward quadrant gets somewhat pronounced as the area ratio and flight velocity increase. All these things,

however, take place along with massloss and thrustloss in an IP-cycle. Thus when an IP-cycle is compared with a CP-cycle, although it looks great and impressive that an IP-cycle is much quieter than a CP-cycle, one must bear in mind that this is unfortunately at the expense of two vital factors that govern the power of the jet. They are the massflow and the thrust. Furthermore, as increased values of outer-to-inner area ratios (Σ) result in increased massloss and thrustloss followed by higer bypass ratios, one should realize that the best noise-optimization in an IP-cycle can be obtained by choosing one with a low bypass ratio operation obtainable at a lower outer-to-inner area ratio (Σ), preferably at $\Sigma = 1$, where it will provide not only the least amount of noise, but also the maximum thrust and massflow.

On the other hand, a VSCE-cycle which maintains a constant massflow and constant thrust in perfect parity with those of a CP-cycle is substantially less noisy than a CP-cycle. As the plots in Figures 3(b)-3(d) show a VSCE-cycle (as compared against a CP-cycle) provides a noise reduction of at least 18.0 dB at $\Sigma = 0.25$, 25 dB at $\Sigma = 0.1$, and 30 dB at $\Sigma = 0.05$; furthermore, unlike the IP-cycle, this amount of noise reduction is very uniformly maintained at all angles around the jet both statically and in flight. It has to be pointed out that as the values of Σ go from $\Sigma = 0.25$, to $\Sigma = 0.1$ to $\Sigma = 0.05$, the net massflow and thrust keep on increasing. Thus if the CP-cycle is interchanged with a VSCE-cycle, we not only maintain the same massflow and thrust constant, we also obtain a tremondous amount of noise reduction uniformly maintained at all angles and at all situations-both statically and in flight. Thus the clear message is that a VSCE-cycle is probably the best engine-cycle that can be conceived of a coaxial configuration which will provide the utmost potential to produce the quietest possible nozzle.

Figure 4 illustrates the change in directional intensity as a result of flight and the comparison is done with respect to the static case when there is no flight so that, $M_f = 0$. The plots show that the flight curves are at a lower level (with respect to the static curves) in the aft quadrant and are at a higher level in the forward quadrant. In other words, flight effects induce reduction of noise in the aft quadrant and amplifiction of noise in the forward quadrant. In addition to these effects, the coalescence of all the static and flight curves at one point implies that there are absolutely no effects due to flight at $\theta = 90°$ to the jet axis. These effects of flight are seen to occur at all values of outer-to-inner area ratios Σ. Moreover, as Σ increases, the level of noise at all angles is enhanced both statically as well as in flight.

Figure 5 shows the change in directional intensity of radiation due to an inverted profile coaxial flow, and the change is shown to have occured as a result of variation outer-to-inner area ratios (Σ) and also as a result of flight. The plots show that as flight Mach number, M_f, increases the parts of the curves in the aft quadrant gradually come down and those in the forward quadrant gradually go up, which implies that flight effects induce reduction of noise in the aft quadrant and amplification of noise in the forward quadrant. Furthermore, when one looks at these plots, one notices that as the outer-to-inner area ratios (Σ) increases, it generates somewhat increased amount of radiation at all angles. However, as a result of increasing values of Σ, the inverted profile unfortunately suffers from gradual massloss and thrustloss. Therefore, an inverted profile can really be functionally and acoustically efficient provided one looks for one with

low outer-to-inner area ratio which in consequence is of a low bypass type, and this can be achieved by choosing one with outer-to-inner area ratio (Σ) equal to unity so that the massflow and thrust are maintained constant and are in perfect parity with respect to those of a conventional profile. These requirements, as indicated earlier, are essential to provide optimization of noise due to an inverted profile coaxial nozzle. The directivities shown in Figure 5 indicate that the intensity is directional with a peak more or less close to the jet axis. As the area ratio (Σ) is increased, the directivity becomes more pronounced and the peak location occurs at angles between 48° to 57° at M_f = 0, between 32° to 45° at M_f = 0.3 and then along the jet axis at M_f = 0.6. Thus we are led to believe that the effects of flight shift the peaks closer to the jet axis in the direction of the nozzle inlet. The amplification from 90° to the peak angle is about 10 dB for Σ = 10, 20, 40, 80 and about 13 dB for Σ = 4 and about 18.5 dB for Σ = 1, at M_f = 0. These differences in peak SPL decrease as the flight Mach number M_f increases.

Figures 6(a-c) show the change in directional intensity and the variation in sound pressure level, SPL (dB), due to coaxial streams where both the streams are unequally heated. These coaxial configurations are termed as: Conventional Turbofan (CT) profile, Duct-Burning (DB) profile and Duct-Burning-cum-Variable Stream Control Engine (DB-VSCE) cycle. A conventional turbofan (CT) profile represents a coaxial configuration where the flow pattern consists of a very hot, high speed inner flow combined with hot, slow speed outer flow (M_p = 0.9, T_1 = 1152°K; M_s = 0.54, T_2 = 576°K in our case). A duct-burning (DB) profile represents a coaxial configuration where the flow pattern consists of a hot, high speed inner flow combined

with a hotter, higher speed outer flow (M_p = 0.9, T_1 = 576°K; M_s = 1.08, T_2 = 1152°K in our case). In going from a conventional turbofan profile to a duct-burning profile, one must notice that the outer-to-inner area ratio (Σ) has been left unchanged. However, in the case of a duct-burning-cum-variable stream control engine cycle, the concept of area inversion has to be included to the duct-burning concept already in vogue to create a DB-VSCE cycle. As one goes from a CT-cycle to a DB-cycle and then to a DB-VSCE cycle, one finds that the massflow and thrust keep on increasing whereas the intensity of radiation keep on decreasing. In other words, a DB-cycle is less noisy than a CT-cycle even at increased massflow and thrust conditions and at Σ = 4 (see Figure 6(a)), it provides a noise reduction of at least 3 dB in the aft quadrant to 5 dB in the forward quadrant, and this benefit in noise reduction due to the DB-cycle is very well maintained both statically and in flight. On the other hand, amongst these three different cycles a DB-VSCE cycle is the least noisy and has the maximum amount of massflow and thrust. The noise reduction due to this (DB-VSCE) cycle with respect to a CT-cycle, at area ratio Σ = 4, is any where between 5 dB in the aft quadrant to nearly 10 dB in the forward quadrant when there is no flight. As flight Mach number M_f increases from M_f = 0.0 (static case) to M_f = 0.3 to M_f = 0.6, the benefit in noise reduction is not only systematically maintained at all angles but also, especially in the forward quadrant, this noise reduction is enhanced from 10 dB to 15 dB. Figure 6(b) shows that at area ratio Σ = 10 and at flight Mach number M_f = 0, the DB-VSCE cycle provides a noise reduction of at least 11.5 dB in the aft quadrant to at least 17.5 dB in the forward quadrant with respect to a CT-cycle. This amount in noise reduction is increased to at least 14 dB in the aft quadrant and to

aleast 18 dB in the forward quadrant due to flight at Mach number M_f = 0.3. As the flight Mach number is further increased to M_f = 0.6, the aft quadrant noise reduction remains more or less stable, but in the forward quadrant the benefit in noise reduction is increased to nearly 20 dB with respect to the CT-cycle. As we go to a higher value of outer-to-inner area ratio as in Figure 6(c), these noise reductions are further enhanced at all angles both statically and in flight, and these benefits accruing from a DB-VSCE cycle are, however, obtained at higher massflow and thrust conditions. Thus as a result of this discussion, it is very clear that amongst these three possible engine cycles where both coaxial streams are unequally heated-CT-cycle, DB-cycle, and DB-VSCE cycle— a DB-VSCE cycle has not only the maximum massflow and thrust, but also is the least noisy both statically and in flight. And the benefit in noise reduciton is systematically maintained and markedly enhanced at all angles as the outer-to-inner area ratio increases.

5. SUMMARY OF THE RESULTS

As a result of this study on the effects of flight on noise from hot coaxial dual flows, we find the following conclusions. Flight effects induce:

i) amplification of noise in the forward quadrant ($\pi/2 \leq \theta \leq \pi$)

ii) reduction of noise in the aft quadrant ($0 \leq \theta \leq \pi/2$) and

iii) absolutely no impact on noise at θ = 90° to the jet axis.

Furthermore, the results of this study show that:

iv) at constant massflow and thrust maintained at an outer-to-inner area ratio (Σ) equal to unity, an inverted profile cycle is, at least 6 dB (SPL), quieter than a conventional profile cycle at all angles both statically and inflight,

v) the static benefit in noise reduction due to an inverted profile is maintained in the aft quadrant, but somewhat lost in the forward quadrant due to flight,

vi) an inverted profile incurs massloss and thrustloss, as the outer-to-inner area ratio ($\Sigma > 1$) increases,

vii) an inverted profile, combined with a low bypass ratio operation obtainable at an outer-to-inner area ratio equal to unity ($\Sigma = 1$), provides the best optimization of noise while still maintaining the constant massflow and thrust in complete parity with a CP-cycle,

viii) amongst all the possible coaxial configurations where one of the streams is heated – conventional profile (CP), inverted profiole (IP), and variable stream control engine (VSCE)-cycle – a VSCE cycle (Figure 3) is the best and the most viable engine cycle insofar as it provides a tremondous amount of noise reduction, with respect to the CP- and IP-cycles, both statically and in flight while absolutely maintaining the constant massflow and thrust as of the CP-cycle,

ix) the noise reduction capability of a VSCE-cycle relative to a CP-cycle dramatically increases from over 18 dB at (an outer-to-inner area ratio) $\Sigma = 0.25$, to 25 dB at $\Sigma = 0.1$, and 30 dB at $\Sigma = 0.05$ at all angles,

x) the noise suppression due to the VSCE-cycle is uniformly maintained to the fullest extent at all static as well as flight conditions,

xi) the massflow and thrust of a VSCE-cycle increase with the decrease in outer-to-inner area ratio (as Σ goes from $\Sigma = 0.25$ to 0.1, 0.05),

xii) a VSCE-cycle is the most effective and efficient concept insofar as it is least noisy and yet provides the maximum massflow and thrust and far superior in quality to an IP-cycle which is substantially noisier than the VSCE-cycle even at much less massflow and thrust conditions,

xiii) at any outer-to-inner area ratio $\Sigma > 1$, a duct-burning cycle (Figure 6) provides more massflow and thrust than a conventional turbofan cycle; yet it is much less noisy than the conventional turbofan cycle,

xiv) the static benefit in noise reduction due to the duct-burning cycle with respect to the conventional turbofan cycle is, at $\theta = 90°$ to the jet axis, around 4 dB at $\Sigma = 4$, 5 dB at $\Sigma = 10$. and 6 dB at $\Sigma = 20$,

xv) the corresponding aft quadrant reductions are slightly less, and the corresponding forward quadrant reductions are somewhat more than the foregoing decibel values,

xvi) the aft quadrant reductions due to the duct-burning cycle obtained statically (with respect to the conventional turbofan cycle) are more or less maintained in flight, but the forward quadrant reductions are enhanced by at least 2 dB due to flight at $M_f = 0.3$ or $M_f = 0.6$,

xvii) in the duct-burning case also, a low bypass ratio operation is most desirable for optimizing noise suppression and maximizing thrust and massflow,

xviii) amongst all the possible coaxial configurations (Figure 6) where both the streams are unequally heated—conventional turbofan (CT) cycle, duct-burning (DB) cycle, and duct-burning-cum-variable stream control

engine (DB-VSCE) cycle—a DB-VSCE cycle provides the maximum massflow and thrust, and yet is the least noisy,

xix) the static benefit in noise reduction due to a DB-VSCE cycle over a CT-cycle is of the order of 5.6 dB to 10 dB at Σ = 0.25, 11 dB to 17.5 dB at Σ = 0.1, and 17.5 dB to 22.5 dB at Σ=0.05, the lower dB-levels ranging over the aft quadrant and the higher dB-levels ranging over the forward quadrant,

xx) the aft quadrant reductions due to the DB-VSCE sycle obtained statically (over the CT-cycle) is well maintained in flight whereas the forward quadrant reductions are somewhat enhanced due to flight,

xxi) the massflow and thrust of a DB-VSCE cycle increase with the decrease in outer-to-inner area ratio (as Σ goes to Σ = 0.25, to 0.1, 0.05),

xxii) a DB-VSCE cycle is far superior to a DB-cycle which is substantially noisier than DB-VSCE cycle even at much less massflow and thrust conditions.

6. CONCLUDING REMARKS

The coaxial jet noise problem has been discussed on the basis of a double vortex-sheet flow model which involves deliberate suppression of inherent instabilities of the flow. The analysis reveals many important features consistent with the familiarly known results of coaxial jet noise.

One of the most striking features obtained as a result of this study is that a variable stream control engine concept combined with an inverted

profile cycle when one of the streams is heated or that combined with a duct-burning turbofan cycle when both the streams are unequally heated are the two most powerful engine cycles at two different operating conditions, which provide the maximum amount of massflow and thrust and yet generate the minimum amount of noise both statically and in flight. Finally, in the opinion of the author, these two coaxial cycles possibly hold the key to our search for the most effective and efficient nozzles in order to usher us to an era of quiet aircraft.

ACKNOWLEDGMENT

The study was conducted as part of NASA Ames program of research into flight effects on jet noise under the NASA Co-operative Agreement Contract NCC 2-75. I am very grateful to David H. Hickey and Adolf Atencio of NASA Ames for their useful discussion and helpful suggestions. My thanks are also due to R. Mani and T.F. Balsa of GE, to M.E. Goldstein of NASA Lewis and M.S. Howe of BBN for the benefit of discussion. My appreciation goes to David G. Crighton of Leeds and K. Karamcheti of Stanford for their interest in this work. I am highly thankful to Yen Liu of Stanford for his invaluable assistance in programming these calculations.

REFERENCES

DOSANJH, D.S., BHUTIANI, P.K., AHUJA, K.K. & BASSIOUNI, M.R., 1976 Supersonic jet noise suppression by coaxial cold/heated jet flows. AIAA Paper no. 76-507.

HOSKINS, R.F., 1979 Generalized Functions. John Wiley & Sons.

MANI, R. 1976a. The influence of jet flow on jet noise. Part 1 The noise of unheated jets. J. Fluid Mech. 73, 753-778.

MANI,R. 1976b The influence of jet flow on jet noise. Part 2. The noise of heated jets. J. Fluid Mech. 73, 779-793.

FIGURE CAPTIONS

Figure 1. Change in directional intensity of different coaxial modes at constant thrust and massflow.

a). area ratio $\Sigma = 1$, $\bar{M} = 0.48$

● : cold inner-cum-cold outer mode, $M_p = 0.48$, $\Gamma = 1.0$, $P_1 = P_2 = 1$.

⊡ : hot inner-cum-hot outer mode, $M_p = 0.95$, $\Gamma = 1.0$, $P_1 = P_2 = 4$.

⊙ : cold inner-cum-hot outer mode, $M_p = 0.5$, $\Gamma = 1.8$, $P_1 = 1$, $P_2 = 4$.

◇ : hot inner-cum-cold outer mode, $M_p = 0.9$, $\Gamma = 5/9$, $P_1 = 4$, $P_2 = 1$.

b). area ratio $\Sigma = 4$, $\bar{M} = 0.46$

● : cold inner-cum-cold outer mode, $M_p = 0.46$, $\Gamma = 1.0$, $P_1 = 1 = P_2$.

⊡ : hot inner-cum-hot outer mode, $M_p = 0.92$, $\Gamma = 1.0$, $P_1 = 4 = P_2$.

⊙ : cold inner-cum-hot outer mode, $M_p = 0.5$, $\Gamma = 1.8$, $P_1 = 1$, $P_2 = 4$.

◇ : hot inner-cum-cold outer mode, $M_p = 0.84$, $\Gamma = 5/9$, $P_1 = 4$, $P_2 = 1$.

c). area ratio $\Sigma = 10$, $\bar{M} = 0.454$

● : cold inner-cum-cold outer mode, $M_p = 0.45$, $\Gamma = 1.0$, $P_1 = 1 = P_2$.

⊡ : hot inner-cum-hot outer mode, $M_p = 0.91$, $\Gamma = 1.0$, $P_1 = 4 = P_2$.

⊙ : cold inner-cum-hot outer mode, $M_p = 0.5$, $\Gamma = 1.8$, $P_1 = 1$, $P_2 = 4$.

◇ : hot inner-cum-cold outer mode, $M_p = 0.83$, $\Gamma = 5/9$, $P_1 = 4$, $P_2 = 1$.

d). area ratio $\Sigma = 20$, $\bar{M} = 0452$

● : cold inner-cum-cold outer mode, $M_p = 0.45$, $\Gamma = 1.0$. $P_1 = 1$

⊡ : hot inner-cum-hot outer mode, $M_p = 0.91$, $\Gamma = 1.0$, $P_1 = 4 = P_2$.

⊙ : cold inner-cum-hot outer mode, $M_p = 0.5$, $\Gamma = 1.8$, $P_1 = 1$, $P_2 = 4$.

◇ : hot inner-cum-cold outer mode, $M_p = 0.82$, $\Gamma = 5/9$, $P_1 = 4$, $P_2 = 1$.

Figure 2. Change in directional intensity of different coaxial modes at variable thrust and massflow, and with constant $M_p = 0.5$, $\Gamma = 1.8$

a). area rato $\Sigma = 1$

● : inner cold-cum-outer cold mode, $\bar{M} = 0.73$, $P_1 = 1 = P_2$

⊡ : inner hot-cum-outer hot mode, $\bar{M} = 0.36$, $P_1 = 4 = P_2$.

⊙ : inner cold-cum-outer hot mode, $\bar{M} = 0.48$, $P_1 = 1$, $P_2 = 4$.

◇ : inner hot-cum-outer cold mode, $\bar{M} = 0.66$, $P_1 = 4$, $P_2 = 1$.

b). area ratio $\Sigma = 4$

● : inner cold-cum-outer cold mode, $\bar{M} = 0.84$, $P_1 = 1 = P_2$.

⊡ : inner hot-cum-outer hot mode, $\bar{M} = 0.42$, $P_1 = 4 = P_2$.

⊙ : inner cold-cum-outer hot mode, $\bar{M} = 0.46$, $P_1 = 1$, $P_2 = 4$.

◇ : inner hot-cum-outer cold mode, $\bar{M} = 0.81$, $P_1 = 4$, $P_2 = 1$.

c). area ratio $\Sigma = 10$

● : inner cold-cum-outer cold mode, $\bar{M} = 0.87$, $P_1 = 1 = P_2$.

⊡ : inner hot-cum-outer hot mode, $\bar{M} = 0.44$, $P_1 = 4 = P_2$.

⊙ : inner cold-cum-outer hot mode, $\bar{M} = 0.45$, $P_1 = 1$, $P_2 = 4$.

◇ : inner hot-cum-outer cold mode, $\bar{M} = 0.86$, $P_1 = 4$, $P_2 = 1$.

d). area ratio Σ = 20

● : inner cold-cum-outer cold mode, $\bar{M}$ = 0.89, $P_1 = 1 = P_2$.

⊡ : inner hot-cum-outer hot mode, $\bar{M}$ = 0.44, $P_1 = 4 = P_2$.

⊙ : inner cold-cum-outer hot mode, $\bar{M}$ = 0.45, $P_1 = 1$, $P_2 = 4$.

◇ : inner hot-cum-outer cold mode, $\bar{M}$ = 0.88, $P_1 = 4$, $P_2 = 1$.

Figure 3(a). Comparison of SPL due to conventional profile (CP), inverted profile (IP) and variable stream control engine (VSCE) cycle, all having the same massflow and thrust: area ratio $\Sigma = 1$.

CP(●): $M_p = 0.9$, $\Sigma = 1$, $\Gamma = 5/9$, $P_1 = 4$, $P_2 = 1$, $\bar{M} = 0.48$.

IP(⊙): $M_p = 0.5$ $\Sigma = 1$, $\Gamma = 1.8$, $P_1 = 1$, $P_2 = 4$, $\bar{M} = 0.48$.

VSCE(◇): $M_p = 0.5$, $\Sigma = 1$, $\Gamma = 1.8$, $P_1 = 1$, $P_2 = 4$, $\bar{M} = 0.48$.

Figure 3(b). Comparison of SPL due to conventional profile (CP), inverted profile (IP) and variable stream control engine (VSCE) cycle, with only CP and VSCE-cycle having the same massflow and thrust; area ratio $\Sigma = 4$.

CP(●): $M_p = 0.9$, $\Sigma = 4$, $\Gamma = 5/9$, $P_1 = 4$, $P_2 = 1$, $\bar{M} = 0.49$.

IP(⊙): $M_p = 0.5$, $\Sigma = 4$, $\Gamma = 1.8$, $P_1 = 1$, $P_2 = 4$, $\bar{M} = 0.46$.

VSCE(◇): $M_p = 0.5$, $\Sigma = 0.25$, $\Gamma = 1.8$, $P_1 = 1$, $P_2 = 4$, $\bar{M} = 0.49$.

Figure 3(c). Comparison of SPL due to conventional profile (CP), inverted profile (IP) and variable stream control engine (VSCE) cycle, with only CP and VSCE-cycle having the same massflow and thrust; area ratio $\Sigma = 10$.

CP(●): $M_p = 0.9$, $\Sigma = 10$, $\Gamma = 5/9$, $P_1 = 4$, $P_2 = 1$, $\bar{M} = 0.50$.

IP(⊙): $M_p = 0.5$, $\Sigma = 10$, $\Gamma = 1.8$, $P_1 = 1$, $P_2 = 4$, $\bar{M} = 0.4548$.

VSCE(◇): $M_p = 0.5$, $\Sigma = 0.1$, $\Gamma = 1.8$, $P_1 = 1$, $P_2 = 4$, $\bar{M} = 0.50$.

Figure 3(d). Comparison of SPL due to conventional profile (CP), inverted profile (IP) and variable stream control engine (VSCE) cycle, with only CP and VSCE-cycle having the same massflow and thrust; area ratio $\Sigma = 20$.

CP(●): $M_p = 0.9$, $\Sigma = 20$, $\Gamma = 5/9$, $P_1 = 4$, $P_2 = 1$, $\bar{M} = 0.50$.

IP(⊙): $M_p = 0.5$, $\Sigma = 20$, $\Gamma = 1.8$, $P_1 = 1$, $P_2 = 4$, $\bar{M} = 0.4525$.

VSCE(◈): $M_p = 0.5$, $\Sigma = 0.05$, $\Gamma = 1.8$, $P_1 = 1$, $P_2 = 4$, $\bar{M} = 0.50$.

Figure 4. Change in directional intensity as a result of flight.

$M_p = 0.5$, $\Gamma = 1.8$, $P_1 = 1$, $P_2 = 4$, $\bar{M} = 0.48$

Figure 5. Change in directional intensity and comparison of SPL of an inverted profile as a result of varying outer-to-inner area ratio (Σ); $M_p = 0.5$, $\Gamma = 1.8$, $P_1 = 1$, $P_2 = 4$.

● : $\Sigma = 1$, $\bar{M} = 0.476$

⊙ : $\Sigma = 4$, $\bar{M} = 0.460$

◈ : $\Sigma = 10$, $\bar{M} = 0.455$

⊡ : $\Sigma = 20$, $\bar{M} = 0.453$

▲ : $\Sigma = 40$, $\bar{M} = 0.4513$

△ : $\Sigma = 80$, $\bar{M} = 0.4510$

Figure 6. Comparison of SPL due to conventional turbofan (CT) cycle, duct-burning (DB) cycle and duct burning-cum-variable stream control engine (DB-VSCE) cycle

a). area ratio $\Sigma = 4$

CT(●): $M_p = 0.9$, $\Sigma = 4$, $\Gamma = 0.6$, $P_1 = 4$, $P_2 = 1$, $\bar{M} = 0.40$

DB(⊙): $M_p = 0.9$, $\Sigma = 4$, $\Gamma = 1.2$, $P_1 = 2$, $P_2 = 4$, $\bar{M} = 0.56$

DB-VSCE(◈): $M_p = 0.9$, $\Sigma = 0.25$, $\Gamma = 1.2$, $P_1 = 2$, $P_2 = 4$, $\bar{M} = 0.62$

b). area ratio Σ = 10

CT(●): M_p = 0.9, Σ = 10, Γ = 0.6, P_1 = 4, P_2 = 2, $\bar{M}$ = 0.389

DB(⊙): M_p = 0.9, Σ = 10, Γ = 1.2, P_1 = 2, P_2 = 4, $\bar{M}$ = 0.55

DB-VSCE(◇): M_p = 0.9, Σ = 0.1, Γ = 1.2, P_1 = 2, P_2 = 4, $\bar{M}$ = 0.628

c). area ratio Σ = 20.

CT(●): M_p 0.9, Σ = 20, Γ = 0.6, P_1 = 4, P_2 = 2, $\bar{M}$ = 0.385

DB(⊙): M_p = 0.9, Σ = 20, Γ = 1.2, P_1 = 2, P_2 = 4, $\bar{M}$ = 0.54

DB-VSCE(◇): M_p = 0.9, Σ = 0.05, Γ = 1.2, P_1 = 2 , P_2 = 4, $\bar{M}$ = 0.632

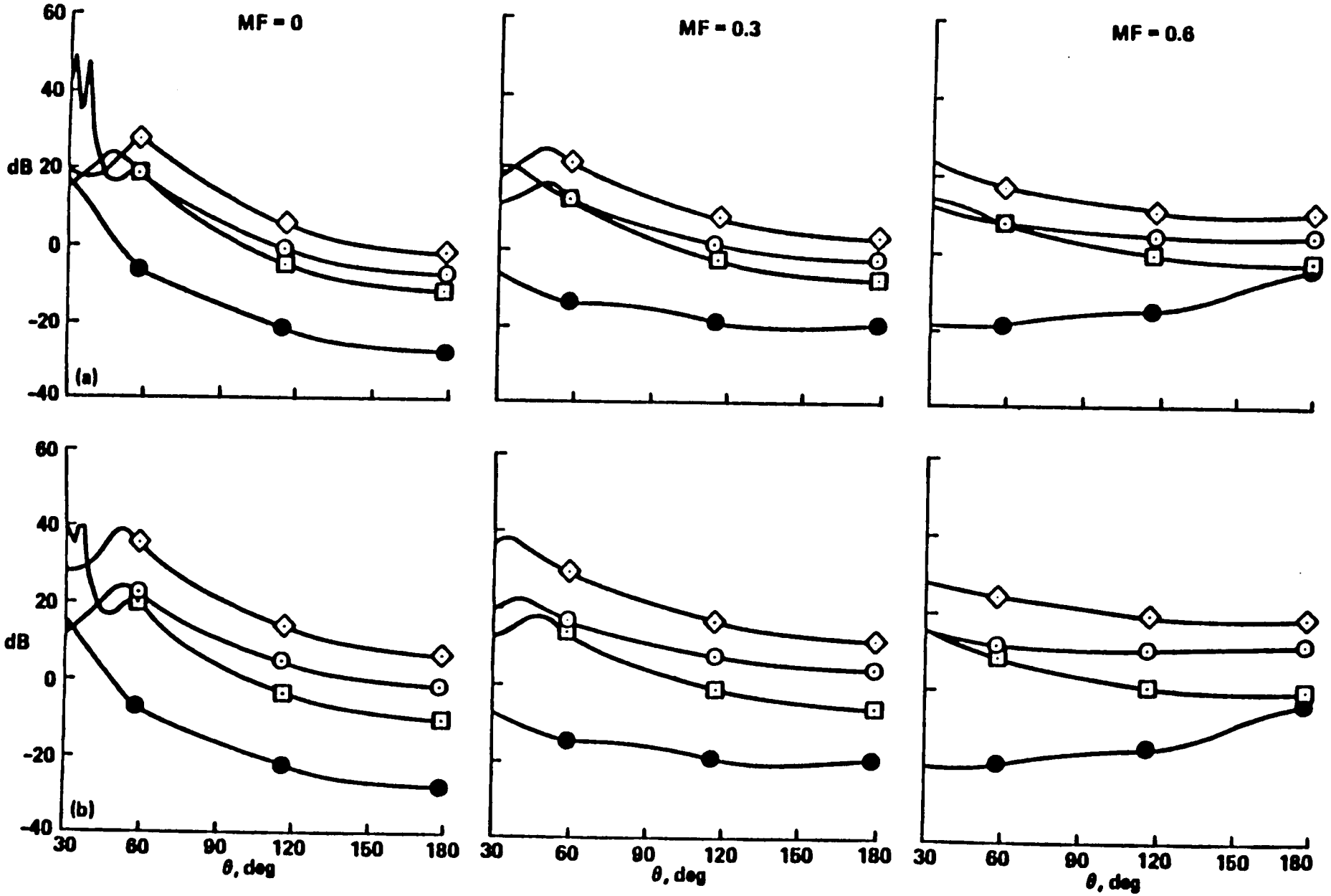

FIGURE 1(a) & (b)

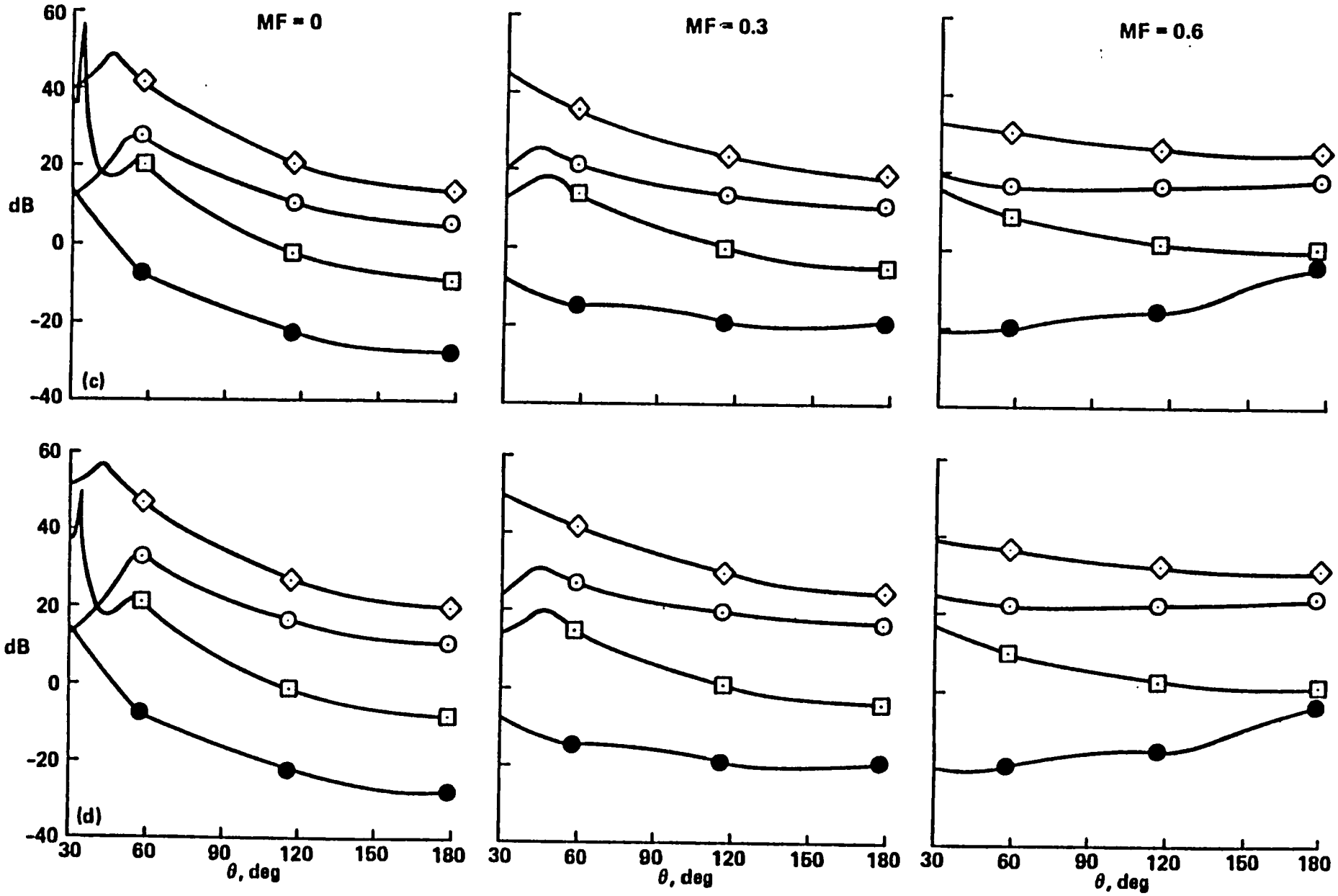

FIGURE 1(c) & (d)

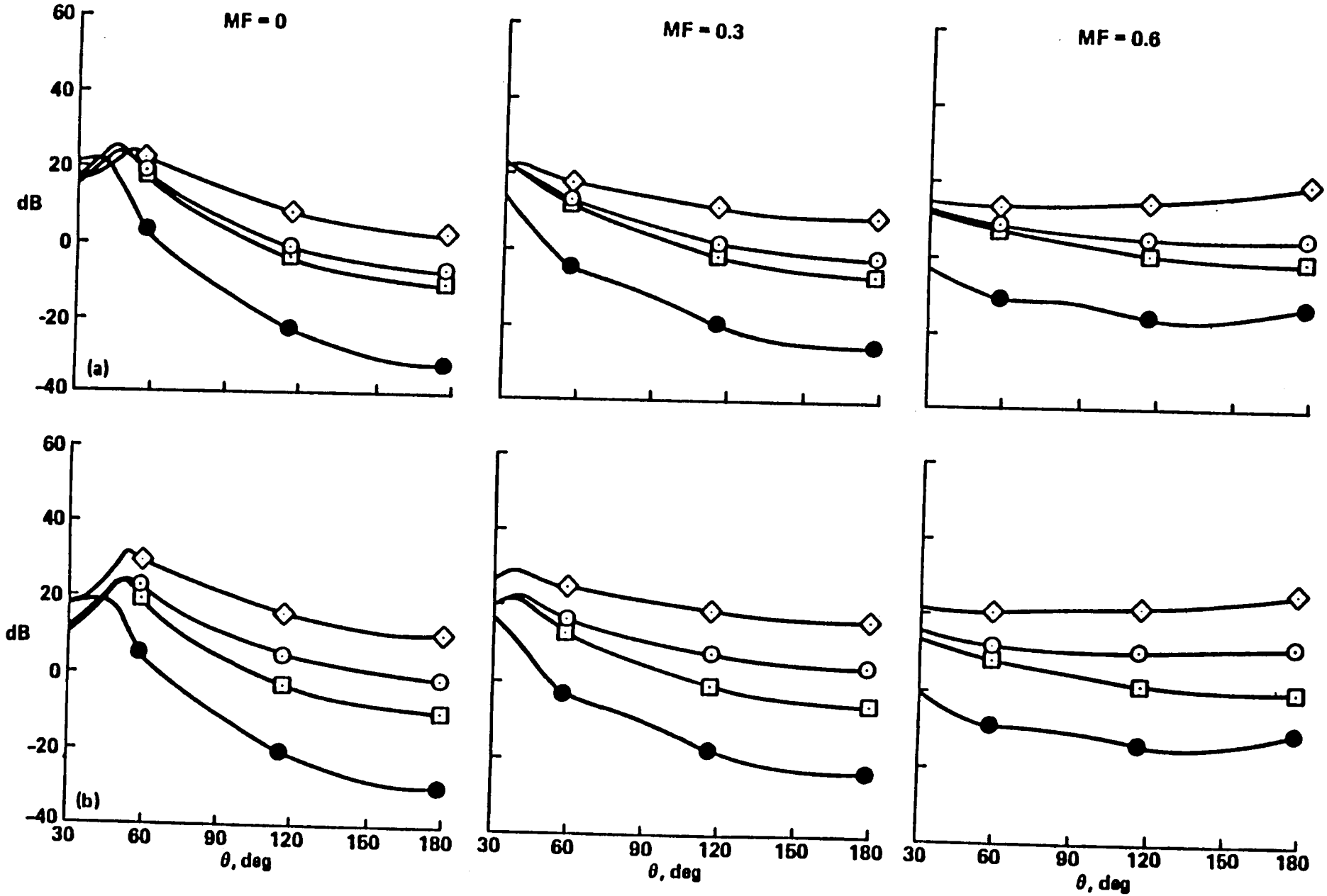

FIGURE 2(a) & (b)

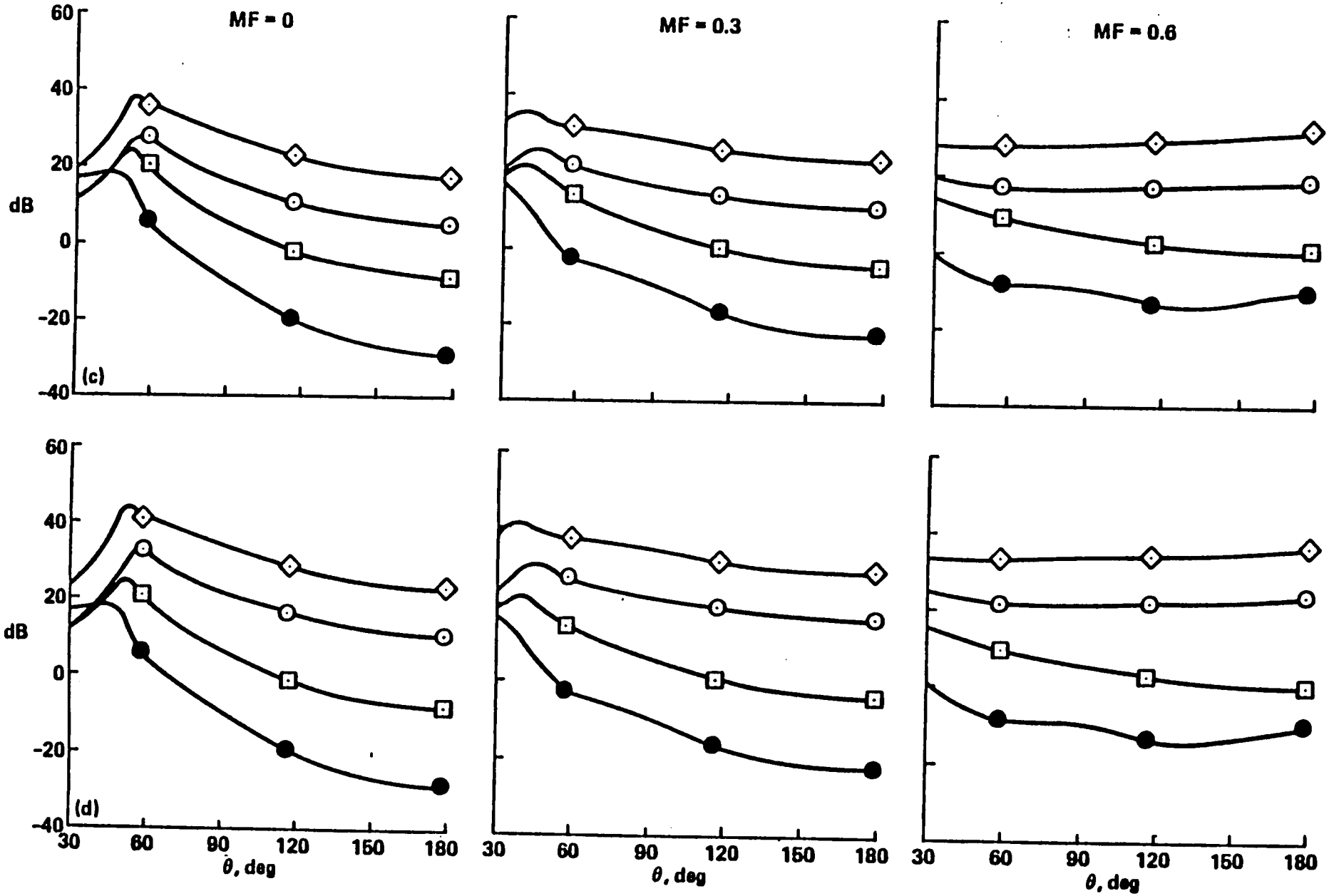

FIGURE 2(c) & (d)

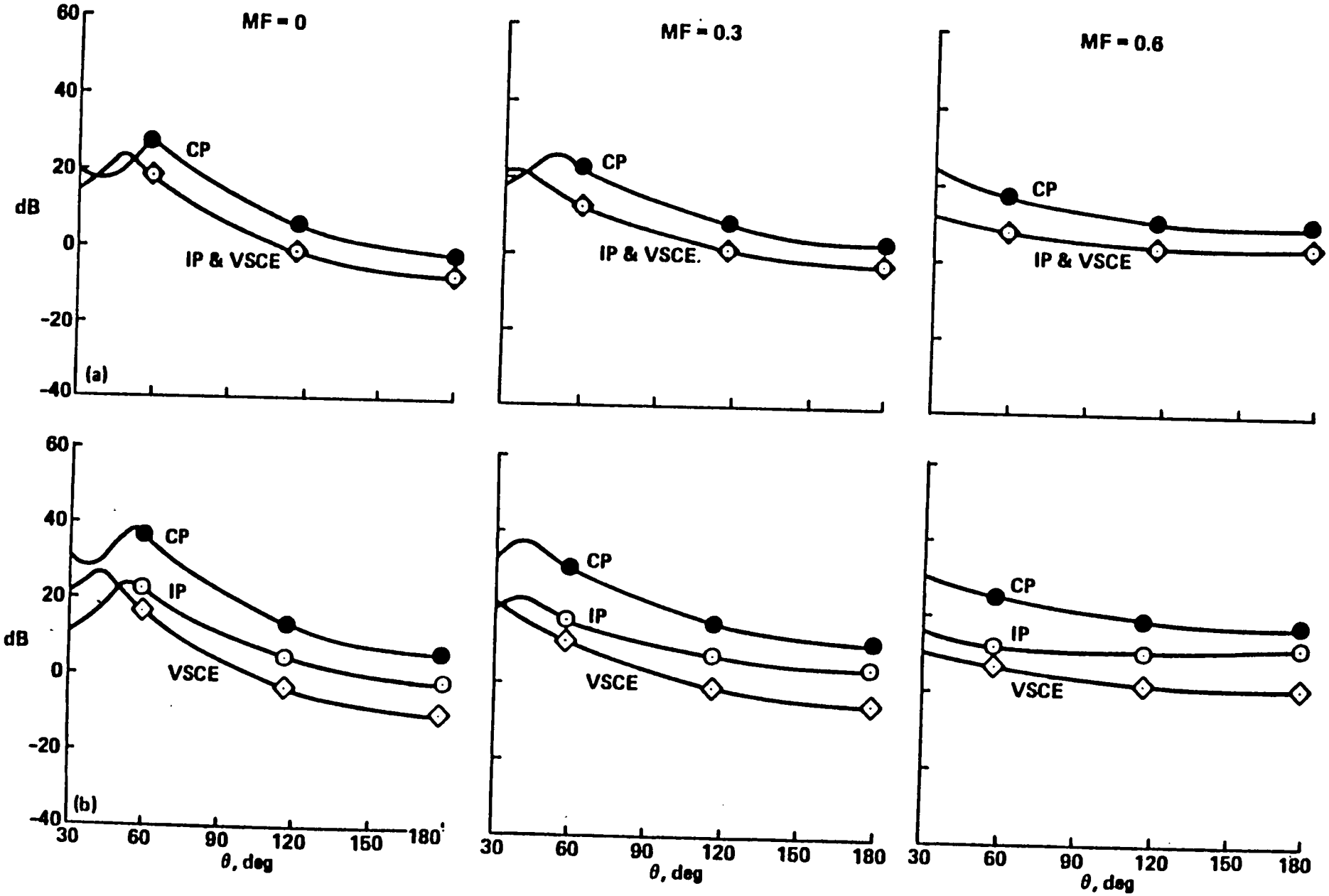
MF = 0
MF = 0.3
MF = 0.6
60
40
20
0
-20
-40
dB
CP
IP & VSCE
(a)
IP
VSCE
(b)
30
60
90
120
150
180
θ, deg

FIGURE 3(a) & (b)

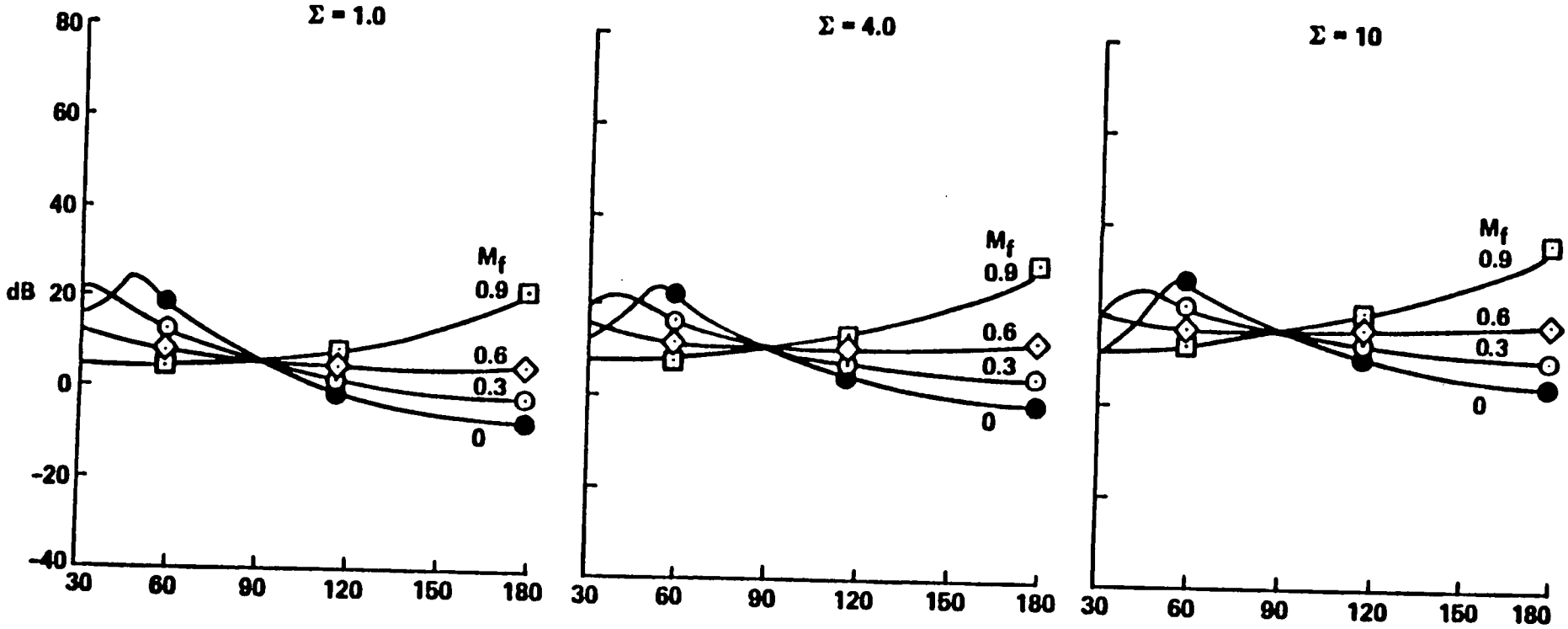

FIGURE 4

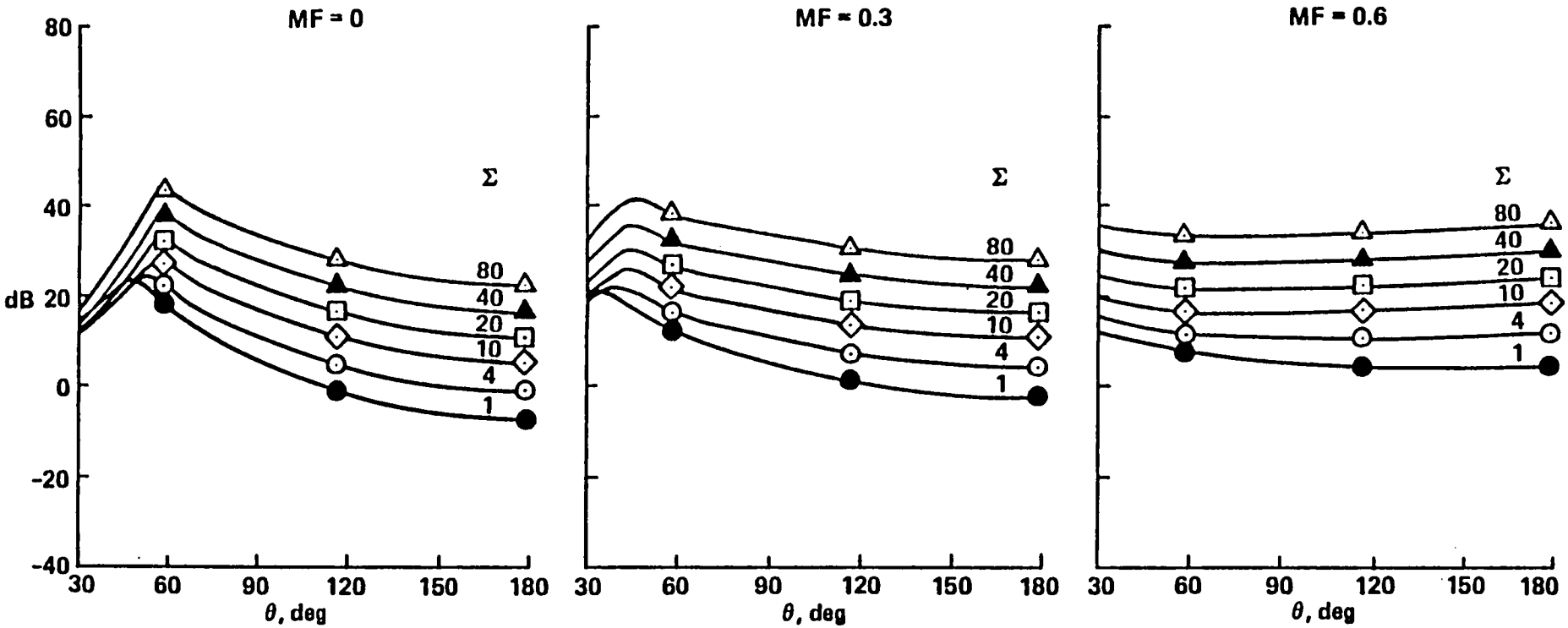
MF = 0
MF = 0.3
MF = 0.6
80
60
40
dB 20
0
-20
-40
Σ
80
40
20
10
4
1
30
60
90
120
150
180
θ, deg

FIGURE 5

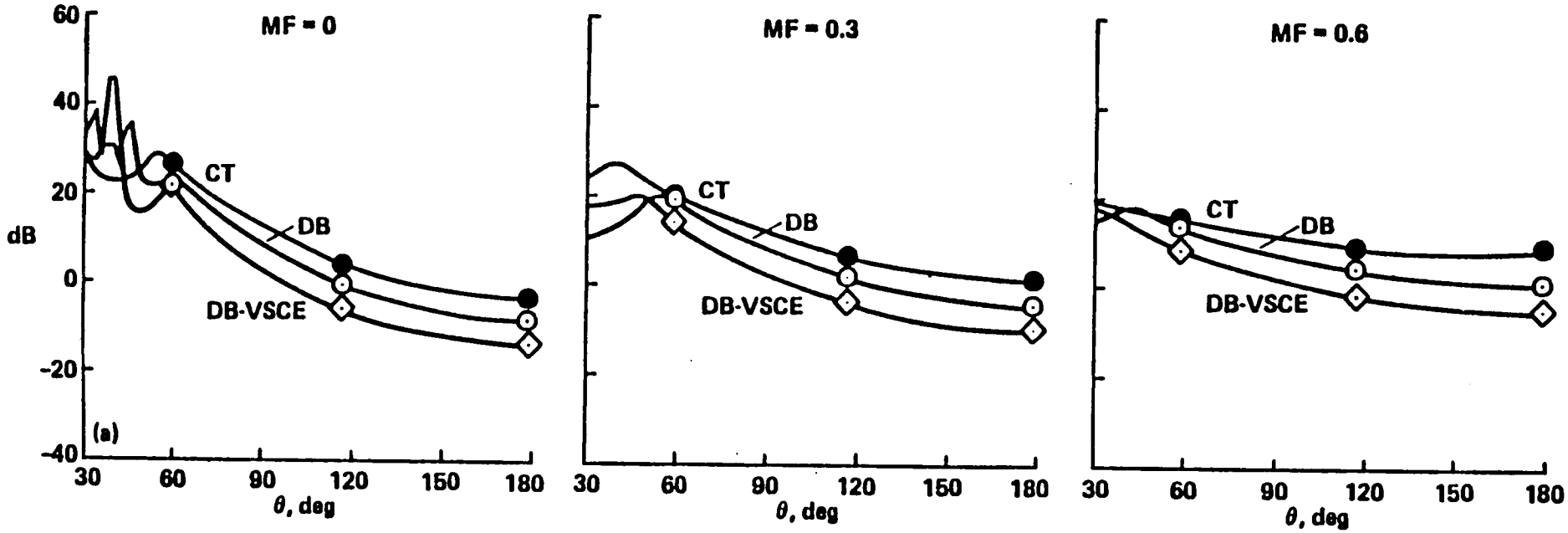
MF = 0
MF = 0.3
MF = 0.6
CT
DB
DB-VSCE
dB
60
40
20
0
-20
-40
(a)
30
60
90
120
150
180
θ, deg

FIGURE 6(a)

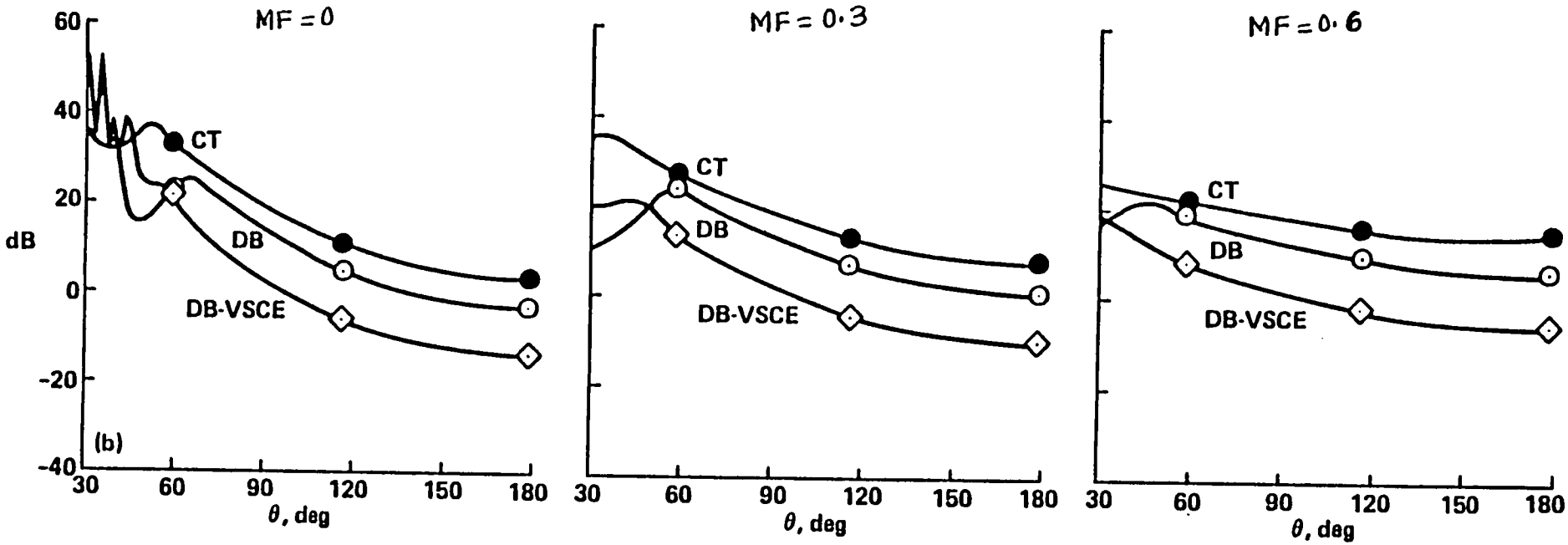
MF = 0
MF = 0.3
MF = 0.6
CT
DB
DB-VSCE
dB
60
40
20
0
-20
-40
(b)
30
60
90
120
150
180
θ, deg

FIGURE 6(b)

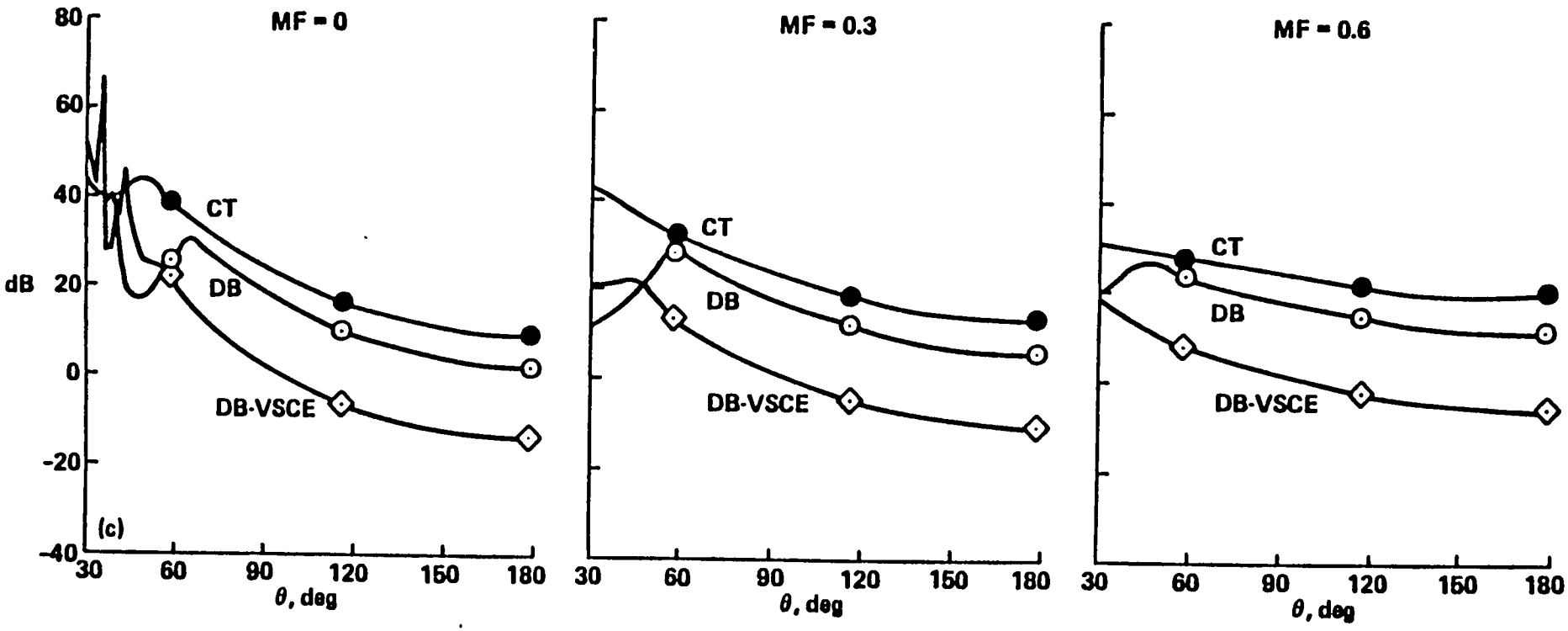
MF = 0
MF = 0.3
MF = 0.6
CT
DB
DB-VSCE
dB
80
60
40
20
0
-20
-40
(c)
30
60
90
120
150
180
θ, deg

FIGURE 6(c)